NRL Report 7977

Airborne Radar Motion Compensation Techniques: Optimum Array Correction Patterns

G. A. ANDREWS, JR.

Airborne Radar Branch
Radar Division

March 16, 1976

NAVAL RESEARCH LABORATORY
Washington, D.C.

SECURITY CLASSIFICATION OF THIS PAGE (When Data Entered)

REPORT DOCUMENTATION PAGE

READ INSTRUCTIONS BEFORE COMPLETING FORM

1. REPORT NUMBER: NRL Report 7977
2. GOVT ACCESSION NO.:
3. RECIPIENT'S CATALOG NUMBER:

4. TITLE (and Subtitle): AIRBORNE RADAR MOTION COMPENSATION TECHNIQUES: OPTIMUM ARRAY CORRECTION PATTERNS.

5. TYPE OF REPORT & PERIOD COVERED: Interim report on a continuing NRL Problem.

6. PERFORMING ORG. REPORT NUMBER:

7. AUTHOR(s): G. A. Andrews, Jr.

8. CONTRACT OR GRANT NUMBER(s): [illegible]A360-0000/058B/ 4F12-141-601, WF12-141

9. PERFORMING ORGANIZATION NAME AND ADDRESS: Naval Research Laboratory, Washington, D.C. 20375

10. PROGRAM ELEMENT, PROJECT, TASK AREA & WORK UNIT NUMBERS: NRL Problem R02-29, Project WF 12-141-601

11. CONTROLLING OFFICE NAME AND ADDRESS: Department of the Navy, Naval Air Systems Command, Washington, D.C. 20361

12. REPORT DATE: March 1976

13. NUMBER OF PAGES: 30

14. MONITORING AGENCY NAME & ADDRESS (if different from Controlling Office): 30 p.

15. SECURITY CLASS. (of this report): Unclassified

15a. DECLASSIFICATION/DOWNGRADING SCHEDULE:

16. DISTRIBUTION STATEMENT (of this Report)

Approved for public release; distribution unlimited.

DDC RECEIVED APR 12 1976 D

17. DISTRIBUTION STATEMENT (of the abstract entered in Block 20, if different from Report)

WF12-141-601

18. SUPPLEMENTARY NOTES

19. KEY WORDS (Continue on reverse side if necessary and identify by block number)

AMTI	Doppler filtering
Airborne moving target indicator	Motion compensation
Antenna pattern	Moving target indicator
Correction pattern	Radar

20. ABSTRACT (Continue on reverse side if necessary and identify by block number)

Moving Target Indicators (MTIs) on moving platforms present a special problem of clutter cancellation because of the motion of the platform in relation to fixed objects. The returns from fixed objects must be filtered out as clutter. A technique was developed for designing antenna correction patterns to minimize clutter residue, averaged over all angles. It is to be used with the Displaced Phase Center Antenna (DPCA) system and can achieve an average clutter cancellation equal to that of an MTI on a stationary platform.

DD FORM 1 JAN 73 1473 EDITION OF 1 NOV 65 IS OBSOLETE S/N 0102-014-6601

SECURITY CLASSIFICATION OF THIS PAGE (When Data Entered)

251 950 LB

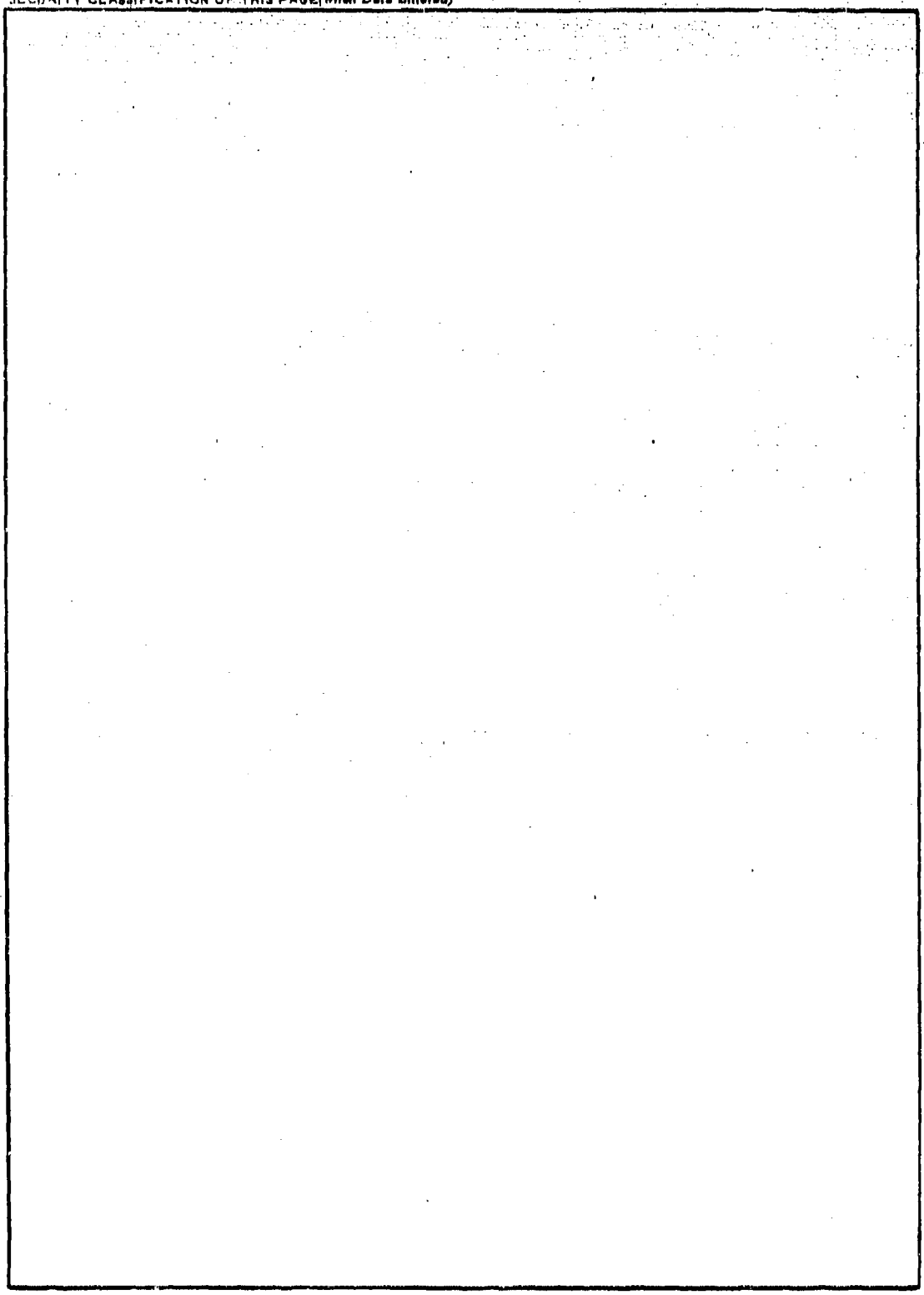

CONTENTS

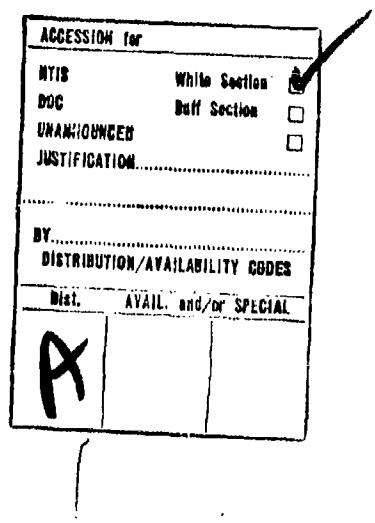

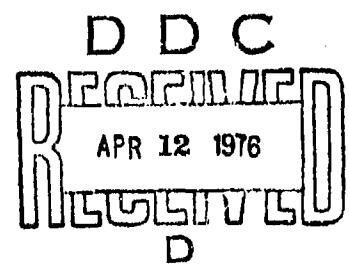

AIRBORNE RADAR MOTION COMPENSATION TECHNIQUES: OPTIMUM ARRAY CORRECTION PATTERNS

INTRODUCTION

The airborne moving target indicator (AMTI) problem is really two problems. Besides the usual MTI problem of designing doppler filters to detect targets of unknown velocity, AMTI design must account for motion of the platform in relation to fixed objects (clutter).

It has been shown [1] that doppler processors can maximize the detection of moving targets if the mean doppler shift of the clutter as well as the shape of the clutter spectrum are known. To achieve maximum detection requires that the mean doppler shift be accounted for in the design of the doppler filters.

The performance of the optimal filters is heavily dependent on the width of the clutter spectrum. Doppler filters can be optimized for a wide clutter spectrum, but the performance of such filters is worse than that of doppler filters optimized for narrower clutter spectra. For this reason, any nonstochastic contributions to spectral width, such as the effects of platform motion, must be removed.

Two systems for compensating platform motion are widely used today. Time Averaged Clutter Coherent Airborne Radar (TACCAR) is a phase-locked system designed by MIT Lincoln Laboratory to remove the average doppler shift of the clutter. In Ref. 2, its limitations and a procedure for overcoming them are presented. The displaced Phase Center Antenna (DPCA) system uses combined antenna/AMTI techniques to remove spectral spreading caused by platform motion [3, 4]. This technique is evaluated in Ref. 5 for a sinc x antenna pattern and a perfect but unrealizable correction pattern. The main problem is the design of the correction pattern. In this report, the relationship between any arbitrary array pattern and the corresponding optimum realizable correction pattern is developed. The relationship is used as the basis of optimum correction patterns for several array patterns, and the performances of these patterns are compared with those of theoretically perfect correction patterns.

STATEMENT OF THE PROBLEM

The effects of platform motion are said to be perfectly corrected when the doppler shifts of the returns from objects located anywhere within the antenna pattern are independent of platform motion. Figure 1 shows the effect of platform motion on the observed clutter spectrum. Figure 1a shows a relatively narrow zero-mean spectrum caused by internal motion of the clutter or by radar instabilities. Figure 1b shows the spectrum

Manuscript submitted January 12, 1976.

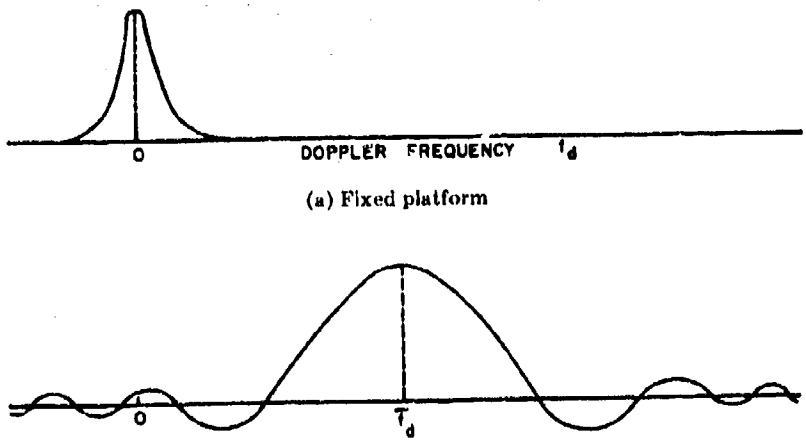

(a) Fixed platform

(b) Moving platform

Fig. 1—Effect of platform motion on the observed clutter doppler spectrum

as received through an antenna on a moving platform. The doppler shift of a finite clutter patch is determined by the platform velocity and the angle between the platform velocity vector and the direction to the clutter patch. The amplitude of the received clutter energy is determined by the angle at which it is received through the antenna pattern. The result is that the mean of the observed spectrum is determined by the pointing angle of the antenna, and its shape by the antenna pattern as shown in Fig. 1b.

TACCAR Correction

If a stationary scatterer is located at an angle (θ_s, ϕ_s) with respect to the aircraft velocity vector v_p, it has an apparent velocity $-v_p$, as shown in Fig. 2.

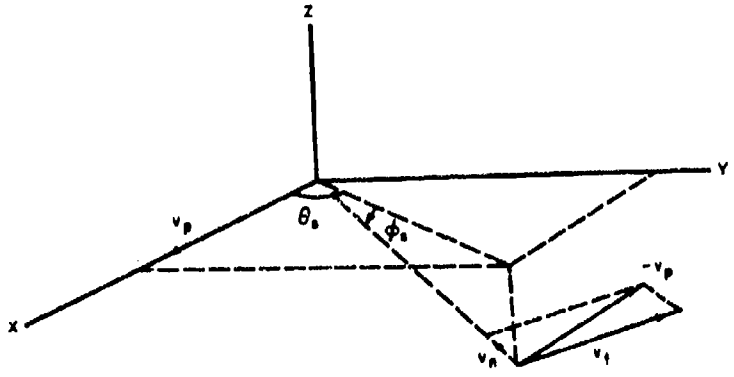

Fig. 2—Velocity relationships [2]

The apparent velocity of the object has a normal component,

$$v_n = -v_p \cos\theta_s \cos\phi_s ,$$

and a tangential component,

$$v_t = -v_p \sin\theta_s \cos\phi_s .$$

The doppler shift of a return from this object is approximately

$$f_d = -2 \frac{v_n}{c} f_t ,$$

where

f_t is transmitted frequency

c is propagation velocity.

If the axis of the antenna pattern is pointing in a direction (θ_a, ϕ_a) with respect to the aircraft velocity vector, and if the object is at an angle (θ, ϕ) to the axis of the antenna pattern, then

$$\theta_s = \theta_a + \theta ,$$

so that

$$v_n = -v_p \cos\phi_s \cos(\theta_a + \theta) ,$$

or

$$f_d = \frac{2v_p}{\lambda} \cos\phi_s (\cos\theta_a \cos\theta - \sin\theta_a \sin\theta) ,$$

where $\lambda = f_t/c$. If we assume isotropic and homogeneous clutter, the doppler shift, averaged over a symmetrical antenna pattern, is

$$\bar{f}_d = f_d|_{\theta=0} = 2 \frac{v_p}{\lambda} \cos\phi_s \cos\theta_a .$$

With TACCAR, $\bar{f}_d$ is estimated and subtracted from f_d to give a corrected doppler of

$$f_d' \doteq f_d - \bar{f}_d ,$$

which when expanded leads to

$$f_d' \doteq 2 \frac{v_p}{\lambda} \cos\phi_s [\cos\theta_a(\cos\theta - 1) - \sin\theta_a \sin\theta] \qquad (1)$$

if the estimate of $\bar{f}_d$ is without error. Reference 2 describes a method for making the error as small as necessary.

The effect of platform motion on the received clutter spectrum was shown in Fig. 1. The result of the TACCAR correction is to shift the spectrum in Fig. 1b to a zero mean value. Remaining is a spectrum, centered at zero doppler frequency, whose shape is determined by the antenna pattern.

Correcting for Spectral Spreading

After the TACCAR correction, an object at angle θ with respect to the center of the antenna pattern has a residual doppler frequency given by Eq. (1). Previously, correction patterns have been designed to correct only over the main lobe of the antenna pattern, and the antenna design has been such that the contribution due to side lobes is small enough to permit the desired radar performance [5]. This report presents a technique for minimizing the total clutter residue averaged over all angles. The number of degrees of freedom for an array pattern design is determined by the number of elements in the array. This procedure uses these degrees of freedom to design for optimal balance between low sidelobes of the correction pattern and accuracy of the pattern over the main lobe.

A 12-element antenna array with omnidirectional elements at 0.5-wavelength spacing was used to illustrate the effect of platform motion on the cancellation of clutter. The pattern for this array is shown in Fig. 3. A Gaussian clutter spectrum is used:

$$W(f) = W_0 \exp(-f^2/2\sigma_c^2) . \tag{2}$$

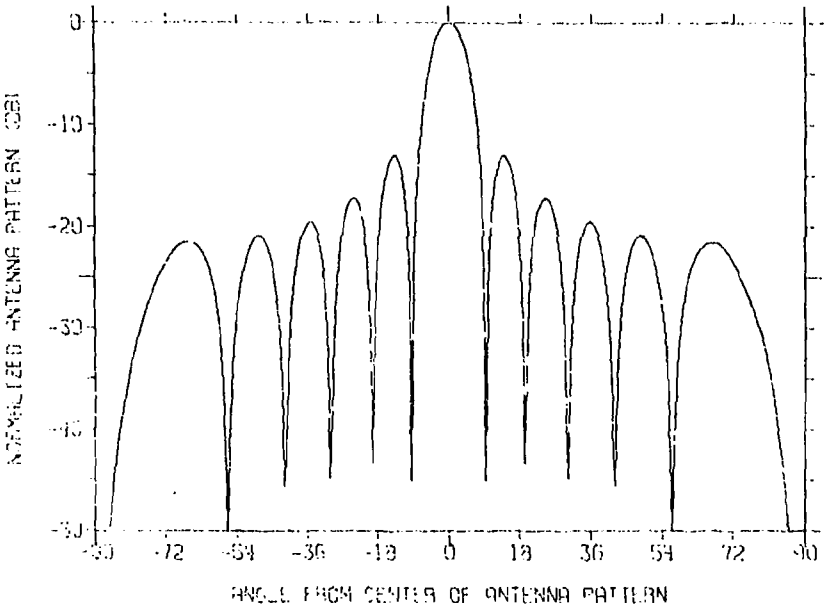

Fig. 3—Mean-squared antenna pattern for a 12-element array with omnidirectional elements at 0.5-wavelength spacing

For isotropic, homogeneous clutter, neither W_0 nor σ_c is a function of the angle with respect to the antenna pattern; σ_c is the standard deviation of the clutter spectrum. The level of clutter power received at an angle θ to the center of the pattern is determined by the two-way antenna power gain at that angle;

$$W(f, \theta) = |G(\theta)|^4 W(f) , \tag{3}$$

where $G(\theta)$ is the antenna pattern. The expression $|G(\theta)|^4$ represents the two-way power gain. This relation between clutter power and angle, when averaged over all frequencies and normalized to the center of the antenna pattern, is illustrated by the curve labeled "input" in Fig. 4.

The cancellation ratio is given by the ratio of input clutter power to output clutter power averaged over all frequencies. The output clutter power for a single canceler is given by

$$C_0(\theta) = 4 \int_{-\infty}^{\infty} \sin^2(\pi f T) W(f, \theta)\, df$$

where T is the reciprocal of the PRF. Since at this point the radar is assumed to be on a stationary platform, only the amplitude, and not the shape, of this spectrum is a function of angle, and the cancellation ratio of an MTI canceler is not a function of the angle.

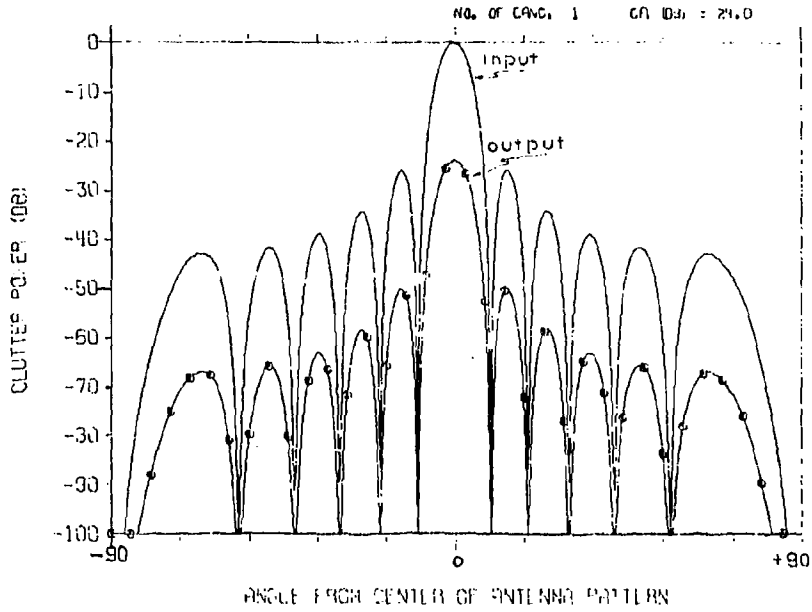

Fig. 4—Clutter power at the input and output of an MTI canceler with no platform motion. The clutter spectral with σ is 0.01 times the radar PRF.

This is demonstrated by the output curve in Fig. 4, which shows a constant 24-dB cancellation ratio when σ_c of Eq. (2) is 0.01 times the pulse repetition frequency (PRF).

When the effect of platform motion is included, the clutter spectra of Eqs. (2) and (3) become

$$W'(f) = W_0 \exp\left[-(f - f_d')^2/2\sigma_c^2\right] \tag{4a}$$

$$W'(f, \theta) = |G(\theta)|^2 W'(f) . \tag{4b}$$

The mean doppler frequency f_d' is given by Eq. (1). The derivative of Eq. (1) with respect to θ is a maximum at $\theta_a = 90°$, assuming that θ is limited to relatively small values, corresponding to the main lobe of the antenna. Therefore the width of the clutter spectrum due to platform motion is a maximum when the antenna is pointing 90° with respect to v_p. The resulting clutter cancellation for this worst case is shown in Fig. 5 for the following conditions:

$$\theta_a = 90°$$

$$v_p \cos \phi_s/\lambda = 0.7 \times \text{PRF}$$

$$\sigma_c = 0.01 \times \text{PRF}.$$

From Fig. 5 we see that at $\theta = 0°$ the cancellation ratio is 24 dB, since f_d' is zero at $\theta = 0$. This is comparable to 24 dB at all angles in Fig. 4 for no platform motion. At other angles, the cancellation of Fig. 5 deteriorates quickly, even becoming negative in the sidelobes.

The average cancellation ratio is given by

$$\text{CR} = \frac{\int_{-\pi}^{\pi} C_i(\theta)\, d\theta}{\int_{-\pi}^{\pi} C_0(\theta)\, d\theta}$$

where

$$C_i(\theta) = \int_{-\infty}^{\infty} W'(f, \theta)\, d\theta$$

$$C_0(\theta) = 4 \int_{-\infty}^{\infty} \sin^2(\pi f T) W'(f, \theta)\, df .$$

The average cancellation ratio is 8.5 dB for the above conditions as compared to 24 dB for no platform motion. The objective is to design an auxiliary antenna pattern that when used with the primary pattern minimizes this loss.

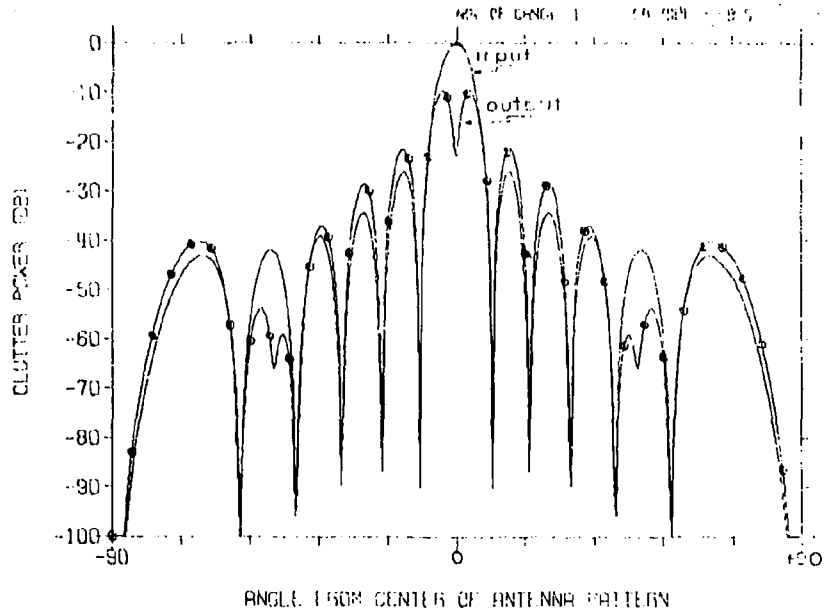

Fig. 5—Clutter at the input and output of an MTI canceler with platform motion. The antenna angle θ_a is 90, σ_c is 0.01 times the pulse repetition frequency, and the velocity factor $v_p \cos \phi_a/\lambda$ is 0.7 times the PRF.

OPTIMAL CORRECTION PATTERNS

Consider an array of elements as shown in Fig. 6–N elements with spacing d and element pattern $E(\theta)$. Let N be any positive, even integer. (Equivalent expressions can be derived for an odd number of elements.)

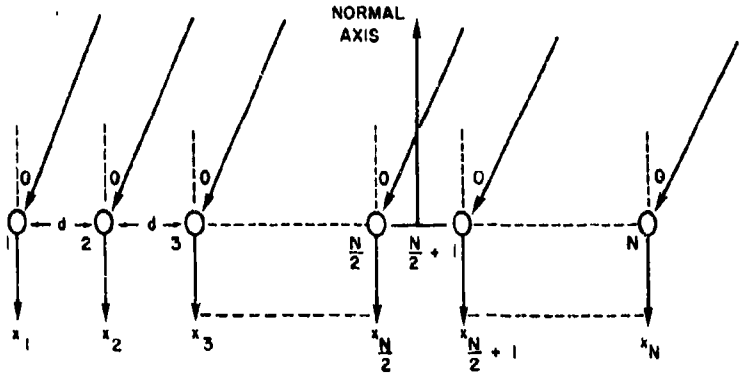

Fig. 6—Antenna array with N elements. Far-field signal is received at an angle θ to the normal axis.

When a signal $v(t)$ is transmitted through a pattern $G_t(\theta)$, reflected by a scatterer located at an angle θ to the normal axis, and received by the N elements of Fig. 6, the received signal at the nth element is

$$x_n = \gamma v(t) G_t(\theta) E(\theta) \exp[j(\omega_s + \omega_p)t] \exp\left[\left(j\,\frac{N+1}{2} - n\right)\phi\right] \tag{5}$$

where $\gamma = Ae^{j\delta}$ represents the unknown amplitude and phase of the received signal, ω_s the doppler shift of the scatterer, and ω_p the doppler shift due to platform motion after the TACCAR correction. Also,

$$\omega_p = 2\pi f_d', \tag{6}$$

where f_d' is given by Eq. (1). The value of ϕ, the phase shift between elements, is given by

$$\phi = \frac{2\pi d}{\lambda} \sin\theta, \tag{7}$$

where λ is the wavelength of the transmitted signal.

The normal receive pattern is defined by a set of weights u_n applied to the outputs of the elements and summed. The signals received through this pattern can be related to the signals of Eq. (5) at each element and the corresponding weights u_n by

$$y_r(t) = \sum_{n=1}^{N} u_n x_n. \tag{8}$$

If the transmitted signal $v(t)$ is a series of radar pulses, the pulse-to-pulse phase advance of the received signal $y_r(t)$ due to platform motion is as shown in Fig. 7.

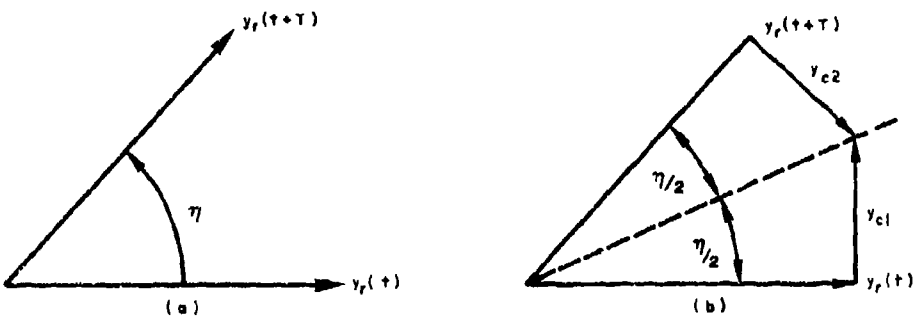

Fig. 7—Phasor representation of (a) pulse-to-pulse advance and (b) platform motion compensation

For each angle θ, the phase advance η is given by

$$\eta = \int_0^T 2\pi f_d' \, dt = \omega_p T , \tag{9}$$

where T is the interpulse period. To correct for this phase advance, correction signals y_{c1} and y_{c2} are added to the received signals, as shown. The objective here is to design an auxiliary array pattern to provide these correction signals. Ideally, the correction would simply result in a phase shift of the received signals for each angle θ across the antenna pattern. Therefore, the desired corrected signals are

$$y_{d1}(t) = \sum_{n=1}^{N} u_n x_n' , \tag{10}$$

where

$$x_n' = x_n e^{+j\omega_p T/2} ; \tag{11}$$

and

$$y_{d2}(t) = \sum_{n=1}^{N} u_n x_n'' , \tag{12}$$

where

$$x_n'' = x_n e^{-j\omega_p T/2} . \tag{13}$$

Adding the correction pattern y_{c1} to $y_r(t)$ yields the actual corrected signal,

$$y = y_r(t) + y_{c1} . \tag{14}$$

The optimal correction pattern is such that the integral

$$I = \int_{-\pi/2}^{\pi/2} |y_{d1} - y|^2 \, d\theta \tag{15}$$

is minimum. The correction signal can be expressed in terms of the weights of the correction pattern as

$$y_{c1} = \sum_{n=1}^{N} b_n' x_n . \tag{16}$$

The weights b_n' for the correction pattern must be selected to minimize Eq. (15). Using matrix notation results in

$$y_r = U_T X = X_T U , \tag{17}$$

where

$$U = \begin{bmatrix} u_1 \\ u_2 \\ \cdot \\ \cdot \\ \cdot \\ u_N \end{bmatrix} \qquad X = \begin{bmatrix} x_1 \\ x_2 \\ \cdot \\ \cdot \\ \cdot \\ x_N \end{bmatrix} ,$$

and T represents the transpose of the matrixes.

$$y_{c1} = B'_T X = X_T B' , \tag{18}$$

where

$$B' = \begin{bmatrix} b'_1 \\ b'_2 \\ \cdot \\ \cdot \\ \cdot \\ b'_N \end{bmatrix}$$

and

$$y_{d1} = U_T X' = X'_T U , \tag{19}$$

where

$$X' = \begin{bmatrix} x'_1 \\ x'_2 \\ \cdot \\ \cdot \\ \cdot \\ x'_N \end{bmatrix} .$$

Using Eqs. (14), (17) and (18) gives

$$y = (U_T + B'_T)X = X_T(U + B') .$$

Expanding the integrand of Eq. (15) results in

$$|y_{d1} - y|^2 = |y_{d1}|^2 + |y|^2 - y^*_{d1} y - y^* y_{d1}$$

$$|y_{d1} - y|^2 = U_T^* X'^* X'^T_T U + (U_T^* + B_T'^*) X^* X_T (U + B)$$
$$- U_T^* X'^* X_T (U + B') - (U_T^* + B_T'^*) X^* X'^T_T U .$$

If the above is integrated with respect to θ, Eq. (15) becomes

$$I = U_T^* P_{x'} U + (U_T^* + B_T'^*) P_x (U + B') - U_T^* P_{x'x} (U + B') - (U_T^* + B_T'^*) P_{xx'} U, \quad (20)$$

where

$P_{x'} = \int_{-\pi/2}^{\pi/2} X'^* X'^T_T \, d\theta$ is the autocorrelation matrix of X'

$P_x = \int_{-\pi/2}^{\pi/2} X^* X_T \, d\theta$ is the autocorrelation matrix of X

$P_{x'x} = \int_{-\pi/2}^{\pi/2} X'^* X_T \, d\theta$ is the cross-correlation matrix of X' and X

$P_{xx'} = \int_{-\pi/2}^{\pi/2} X^* X'^T_T \, d\theta$ is the cross-correlation matrix of X and X'.

From the above equations it can be seen that both autocorrelation matrixes are hermitian; that is,

$$\left.\begin{aligned} (P_{x'})_T^* &= P_{x'} \\ (P_x)_T^* &= P_x \end{aligned}\right\} . \quad (21)$$

Also, the cross-correlation matrixes have the following relationship:

$$(P_{x'x})_T^* = P_{xx'} . \quad (22)$$

The integral I is a minimum if

$$\left.\begin{aligned} \frac{\delta I}{\delta b_n'} &= 0 \\ \frac{\delta I}{\delta b_n'^*} &= 0 \end{aligned}\right\} \text{ for all } n .$$

Differentiating Eq. (20) with respect to b_n' and setting the result equal to zero leads to

$$(U_T^* + B_T'^*)P_x - U_T^* P_{x'x} = 0 . \tag{23}$$

Differentiating Eq. (20) with respect to $b_n'^*$ leads to

$$P_x(U + B') - P_{xx'}U = 0 . \tag{24}$$

By taking the transposed complex conjugate of Eq. (23) and using Eqs. (21) and (22), one obtains Eq. (24). Therefore Eqs. (23) and (24) are redundant and only one is needed. If Eq. (24) is used the optimum weight vector is

$$P_x B'_{\text{opt}} = (P_{xx'} - P_x)U . \tag{25}$$

Equation (25) gives the relationship necessary for computing the optimum correction pattern. Simplification of this equation follows.

The element (n_1, n_2) of the autocorrelation matrix P_x is

$$p_x(n_1, n_2) = \int_{-\pi/2}^{\pi/2} x_{n_1}^* x_{n_2} \, d\theta .$$

Using Eq. (5) yields

$$p_x(n_1, n_2) = |\gamma|^2 |v(t)|^2 \int_{-\pi/2}^{\pi/2} |G_t(\theta)|^2 |E(\theta)|^2 e^{j(n_1 - n_2)\phi} \, d\theta$$

$$= |\gamma|^2 |v(t)|^2 m_x(n_1, n_2) , \tag{26}$$

where $m_x(n_1, n_2)$ is recognized as an element of a covariance matrix if

$$\int_{-\pi/2}^{\pi/2} |G_t(\theta)|^2 |E(\theta)|^2 \, d\theta = 1 . \tag{27}$$

In the same way, element (n_1, n_2) of the cross-correlation matrix $P_{xx'}$ is

$$p_{xx'}(n_1, n_2) = |\gamma|^2 |v(t)|^2 m_{xx'}(n_1, n_2) , \tag{28}$$

where

$$m_{xx'}(n_1, n_2) = \int_{-\pi/2}^{\pi/2} |G_t(\theta)|^2 |E(\theta)|^2 e^{j\omega_b T/2} e^{j(n_1 - n_2)\phi} \, d\theta . \tag{29}$$

Equation (29) represents an element of the cross-covariance matrix under the constraint of Eq. (27). If Eqs. (26) and (28) are used, Eq. (25) becomes

$$M_x B'_{opt} = (M_{xx'} - M_x) U$$

or

$$B'_{opt} = (M_x^{-1} M_{xx'} - I) U . \tag{30}$$

Equation (30) is the desired relationship for the weight vector of the optimum correction pattern. The vector U is the weight vector corresponding to the normal receive pattern. The covariance matrix M_x is computed from

$$m_x(n_1, n_2) = \int_{-\pi/2}^{\pi/2} |G_t(\theta)|^2 |E(\theta)|^2 e^{j(n_1 - n_2)\phi} d\theta . \tag{31}$$

The cross-covariance matrix $M_{xx'}$ is defined by Eq. (29).

The optimum weight vector for the second correction pattern y_{c2} of Fig. 7 can be derived in the same way. This leads to

$$B''_{opt} = (M_x^{-1} M_{xx''} - I) U , \tag{32}$$

where the cross-covariance matrix $M_{xx''}$ is computed from

$$m_{xx''}(n_1, n_2) = \int_{-\pi/2}^{\pi/2} |G_t(\theta)|^2 |E(\theta)|^2 e^{-j\omega_p T/2} e^{j(n_1 - n_2)\phi} d\theta . \tag{33a}$$

Then

$$y_{c2} = \sum_{n=1}^{N} b''_n x_n . \tag{33b}$$

These two correction patterns minimize the effects of platform motion on an MTI canceler.

EFFECTS OF OPTIMAL PATTERNS ON MTI PERFORMANCE

The following four examples illustrate the technique for designing platform motion-correction patterns. The first is the sinc x pattern in Fig. 3. The second uses 12 omnidirectional elements at 0.5-wavelength spacing and 34-dB Tschebychev weights. The third uses 12 dipole elements with 0.9-wavelength spacing and 34-dB Tschebychev weights. The fourth uses 64 dipole elements with 0.5-wavelength spacing and 34-dB Tschebychev weights. In all four cases, the same pattern is used for both transmit and receive. The total receive patterns will consist of these patterns plus the correction patterns defined by Eqs. (30) and (32).

Pattern I

This pattern (Fig. 3) is characterized by an array of 12 omnidirectional elements at 0.5-wavelength spacing. The weights for the normal receive pattern are uniform, so that

$$u_i = 1.0, \quad i = 1, 2, 3, \ldots, N.$$

Using Eq. (30), we compute weights for the first optimum correction pattern for the following parameters:

$$\theta_a = 90^\circ$$

$$v_p \cos \phi_s / \lambda = 0.7 \times \text{PRF}. \tag{34}$$

The resulting weights are real:

$$B'_{\text{opt}} = \begin{bmatrix} 0.935 \\ 0.404 \\ -0.200 \\ 0.134 \\ -0.103 \\ 0.0869 \\ -0.0789 \\ 0.0779 \\ -0.0869 \\ 0.124 \\ -0.363 \\ -1.210 \end{bmatrix}. \tag{35}$$

These weights determine the correction pattern whose amplitude and phase characteristics are shown in Fig. 8. When the weights B''_{opt} for the second correction pattern are computed in the same way; they are found to be related to the weights B'_{opt} as follows:

$$b''_i = b'_{N-i+1}, \quad i = 1, 2, \ldots, N.$$

The amplitude characteristics of the two patterns are the same and are shown in Fig. 8. The phase characteristics of the two patterns are different, but the second is very nearly the negative of the first in phase.

These two patterns are used to correct an MTI canceler, as shown in Fig. 9. When Gaussian clutter defined by Eq. (4) and

$$\sigma_c = 0.01 \times \text{PRF} \tag{36}$$

is applied to the input of this canceler, the relation of clutter cancellation to angle is as plotted in Fig. 10. Comparing Fig. 10 with Fig. 4, which shows the results neglecting platform motion, demonstrates that the motion compensation technique allows about 24 dB of clutter cancellation in the antenna main lobe. This corresponds to 24 dB at all angles in Fig. 4. Therefore, there is no loss in main-lobe clutter cancellation if platform motion is compensated for in this way. However, the output clutter level in the sidelobes (Fig. 10) is actually higher than the input clutter level. This results in an average clutter cancellation ratio of 19.6 dB (a loss of about 4.4 dB). Comparing Fig. 10 with Fig. 5, which shows the results with no compensation, reveals that the total cancellation ratio is improved by 11.1 dB. The 19.6-dB cancellation ratio is a maximum for the selected parameters, and the loss of 4.4 dB results from sidelobe clutter.

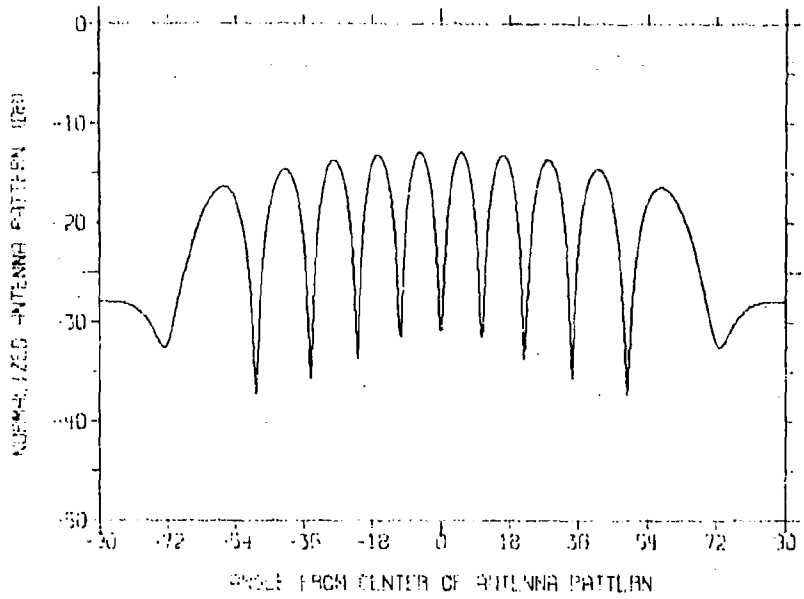

Fig. 8a—Amplitude of the optimum platform motion correction pattern for the antenna pattern of Fig. 3 and the parameters of Eq. (34)

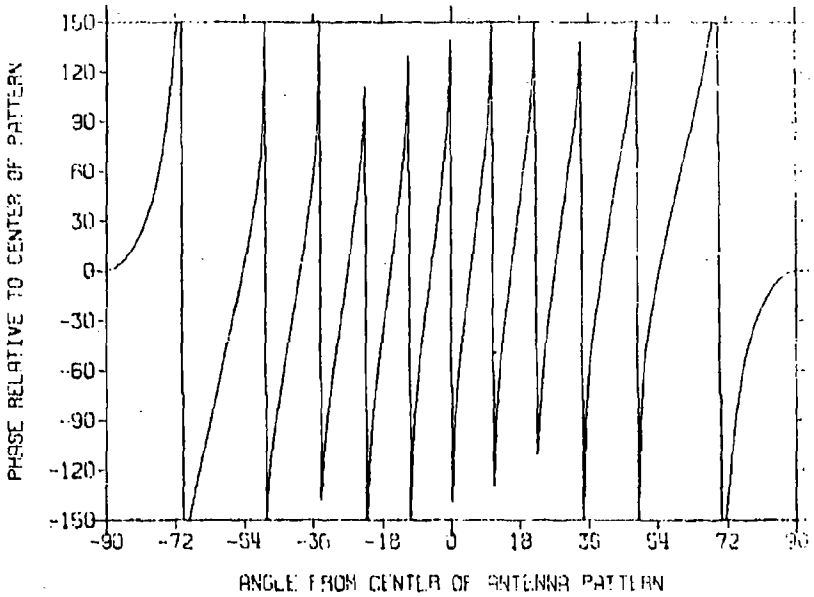

Fig. 8b—Phase of the optimum platform motion correction pattern for the antenna pattern of Fig. 3 and the parameters of Eq. (34)

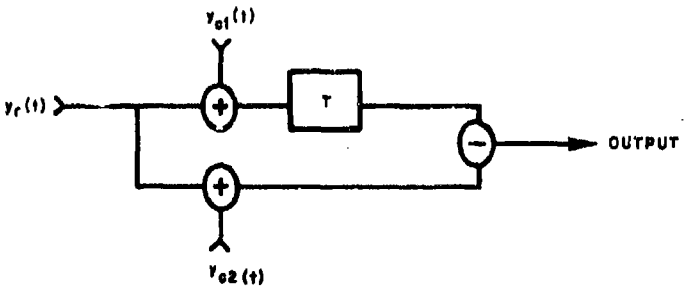

Fig. 9—MTI canceler with platform motion compensation using the correction patterns defined by the weight vectors B'_{opt} and B''_{opt}

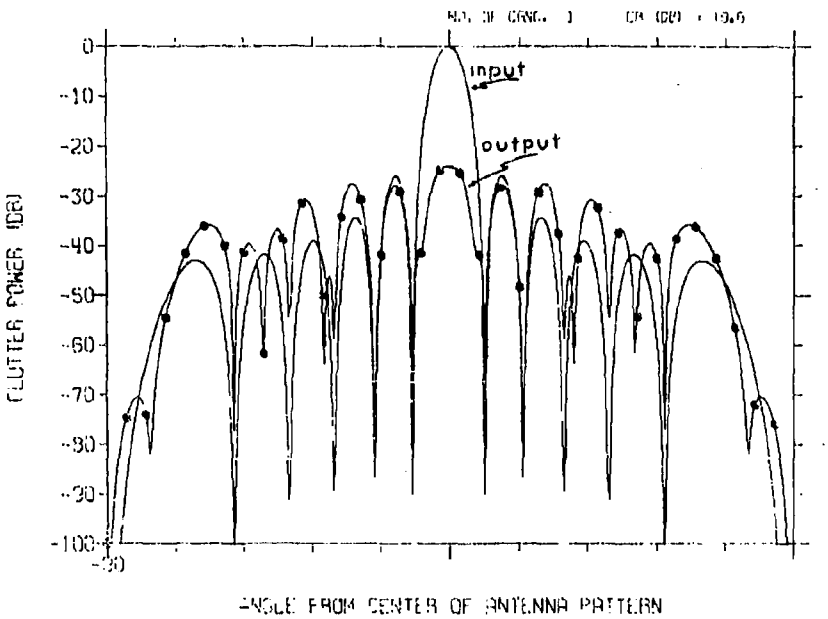

Fig. 10—Clutter power at the input and output of an MTI canceler with platform motion compensation using the correction pattern of Fig. 8 and the system parameters given by Eqs. (34) and (36)

Pattern II

This pattern uses the same array of omnidirectional elements as the one shown in Fig. 3 except that the following 34-dB Tschebychev weights are used:

$$U = \begin{bmatrix} 0.1871 \\ 0.3227 \\ 0.5251 \\ 0.7324 \\ 0.9033 \\ 1.0000 \\ 1.0000 \\ 0.9033 \\ 0.7324 \\ 0.5251 \\ 0.3227 \\ 0.1871 \end{bmatrix}. \tag{37}$$

Using this pattern (Fig. 11) for transmit and receive and using the parameters of Eq. (34), one can compute the weights for the first optimum correction pattern from Eq. (30). They are

$$B'_{\text{opt}} = \begin{bmatrix} 0.628 \\ 0.360 \\ 0.0269 \\ 0.113 \\ 0.102 \\ 0.0925 \\ -0.0852 \\ -0.231 \\ -0.363 \\ -0.300 \\ -0.155 \\ -0.200 \end{bmatrix}. \tag{38}$$

The amplitude and phase characteristics of this correction pattern are shown in Fig. 12. The weights B''_{opt} for the second correction pattern are given by

$$b''_i = b'_{N-i+1}, \quad i = 1, 2, 3, \ldots, N.$$

When these two patterns are used to correct an MTI canceler (see Fig. 9), with Gaussian clutter defined by Eqs. (4) and (36), the clutter cancellation vs angle relationship is as shown in Fig. 13. From Fig. 13, we see that again the 24-dB cancellation ratio is achieved in the main lobe, but output clutter is increased in the sidelobes. Since the sidelobes are much lower than the main lobe for this pattern, they contribute very little to the average, and the average cancellation ratio is about 24-dB, the same as for no platform motion. For this case then, there is an insignificant loss in average clutter cancellation due to platform motion, even though sidelobe clutter is increased.

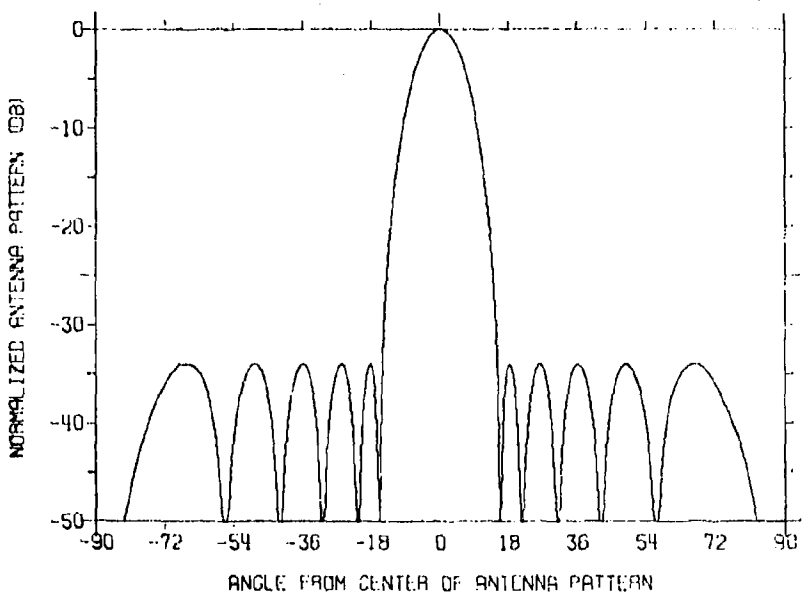

Fig. 11—Mean-squared antenna pattern for a 12-element array with omnidirectional elements at 0.5-wavelength spacing and 34-dB Tschebychev weights

Pattern III

For this pattern, element spacing is increased to 0.9 wavelength, and a dipole element pattern and 34-dB Tschebychev weights are used. The resulting pattern is shown in Fig. 14. The corresponding weights for the correction patterns, using the parameters of Eq. (34), are

$$B'_{\text{opt}} = \begin{bmatrix} 0.315 \\ 0.160 \\ 0.0931 \\ 0.0934 \\ 0.0901 \\ 0.0439 \\ -0.0419 \\ -0.133 \\ -0.189 \\ -0.184 \\ -0.0789 \\ -0.171 \end{bmatrix} \tag{39}$$

and

$$b''_i = b'_{N-1+1} . \tag{40}$$

The amplitude and phase characteristics of this correction pattern (Eq. (39)) are shown in Fig. 15. An MTI canceler with input Gaussian clutter defined by Eqs. (4) and

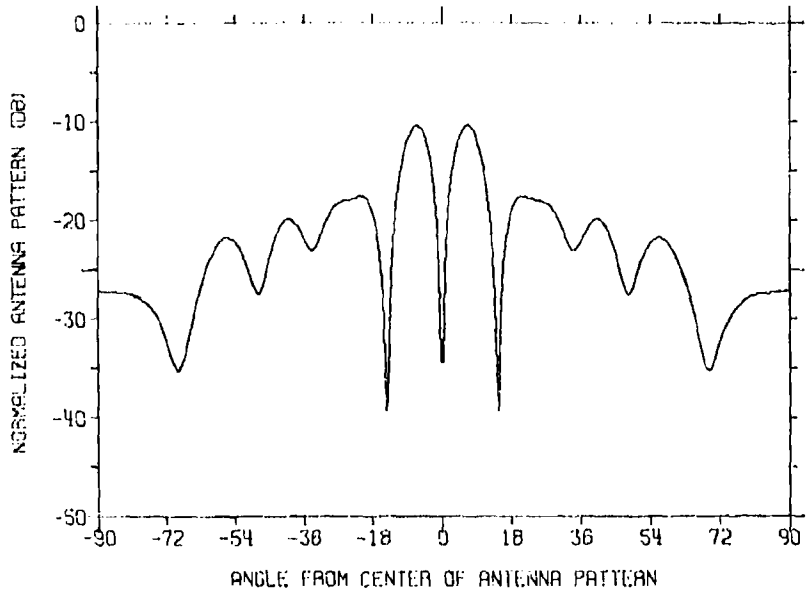

Fig. 12a—Amplitude of the optimum platform motion correction pattern for the antenna pattern of Fig. 11 and the parameters of Eq. (34)

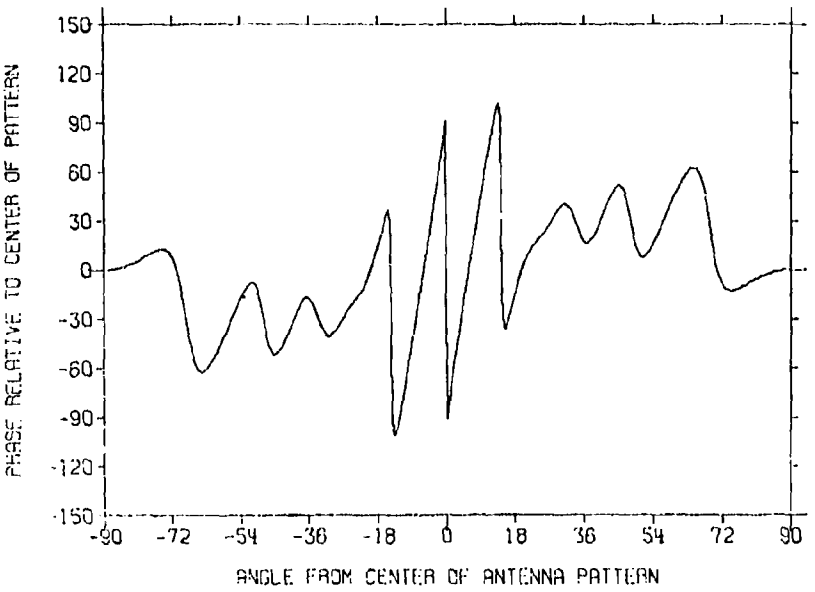

Fig. 12b—Phase of the optimum platform motion correction pattern for the antenna pattern of Fig. 11 and the parameters of Eq. (34)

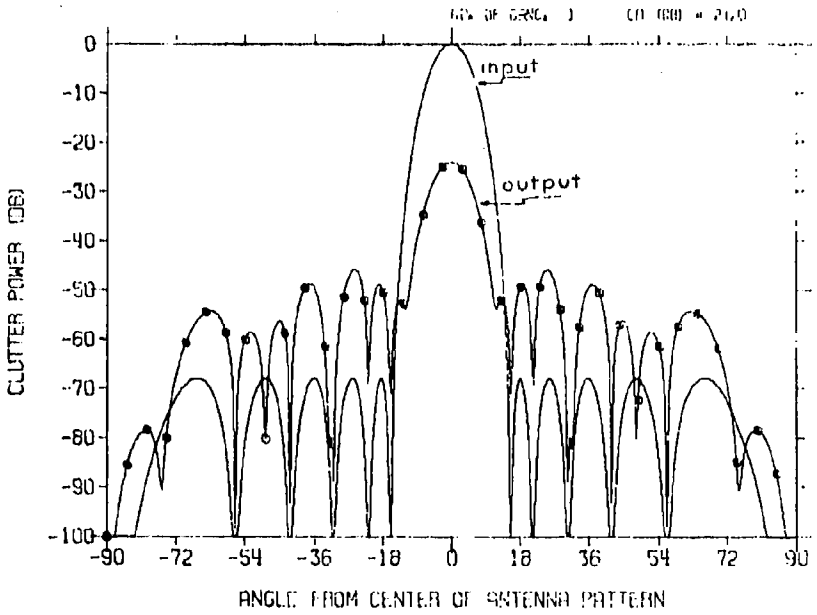

Fig. 13—Clutter power at the output and input of an MTI canceler with platform motion compensation using the correction pattern of Fig. 12 and the system parameters of Eqs. (34) and (36)

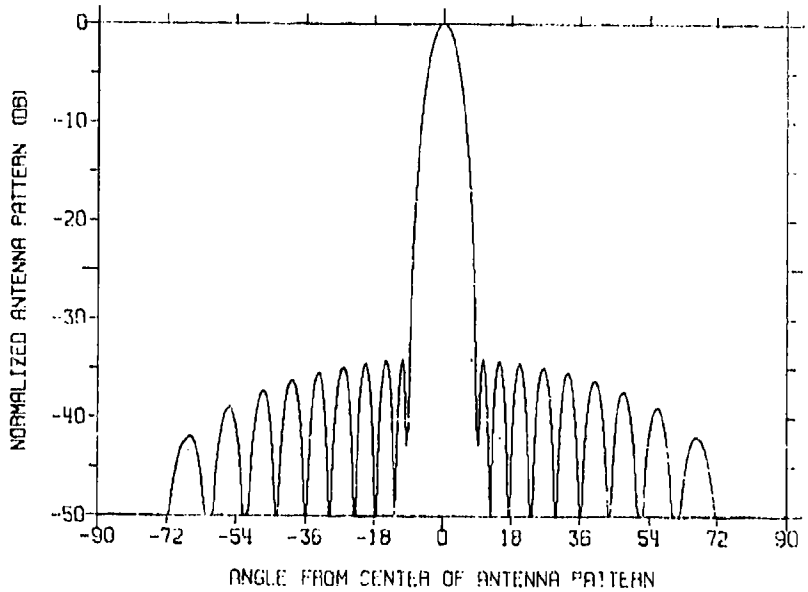

Fig. 14—Mean-squared antenna pattern for a 12-element array with dipole elements at 0.9-wavelength spacing and 34-dB Tschebyschev weights

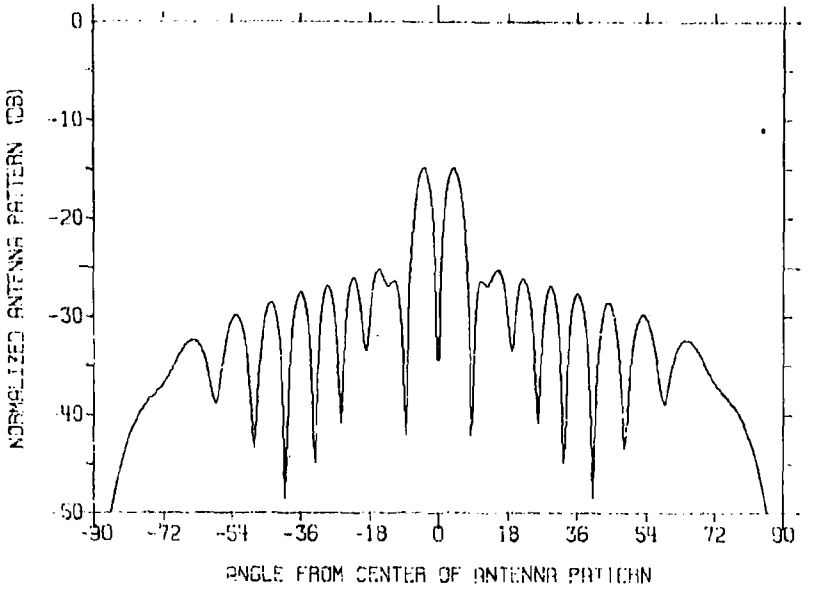

Fig. 15a—Amplitude of the optimum platform motion correction pattern for the antenna pattern of Fig. 14 and the parameters of Eq. (34)

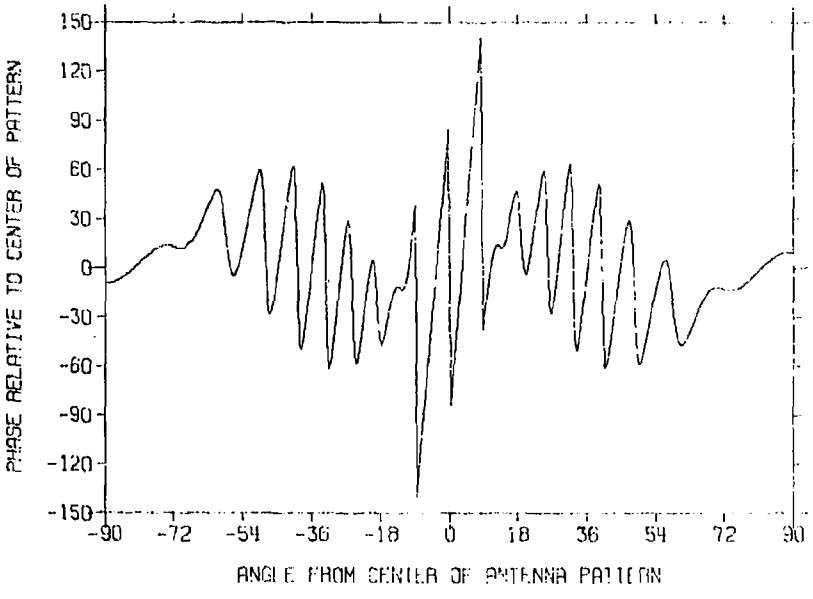

Fig. 15b—Phase of the optimum platform motion correction pattern for the antenna pattern of Fig. 14 and the parameters of Eq. (34)

(36) rejects this clutter as shown in Fig. 16. As with patterns I and II, the loss in mainlobe clutter cancellation is insignificant, but sidelobe clutter level increases. However, because of the low sidelobe level, the loss in average clutter cancellation is again insignificant.

The total input clutter to the MTI canceler is the sum of the clutter from the receive antenna pattern plus that from the correction pattern. In Fig. 16, the cancellation is referred only to the receive pattern clutter. By coherently adding additional clutter in a methodical way, we have shown that the output clutter level can be decreased. Figure 17 shows the sum of the receive pattern (Fig. 14) and the correction pattern (Fig. 15). The sidelobes are at about the −25-dB level; therefore sidelobe clutter is at about the −50-dB level. However, the canceled sidelobe clutter of Fig. 16 is at about the −60-dB level. Therefore there is about 10 dB of sidelobe clutter cancellation, but not enough to overcome the additional sidelobe clutter from the correction pattern.

Pattern IV

The last pattern to be considered is shown in Fig. 18. An array of 64 dipole elements at 0.5-wavelength spacing and with 34-dB Tschebychev weights is used. From Eq. (30), the weights for the first correction pattern are computed for the following parameters:

$$\theta_a = 90^\circ$$
$$v_p \cos\phi_s/\lambda = 2.4 \times \text{PRF}. \tag{41}$$

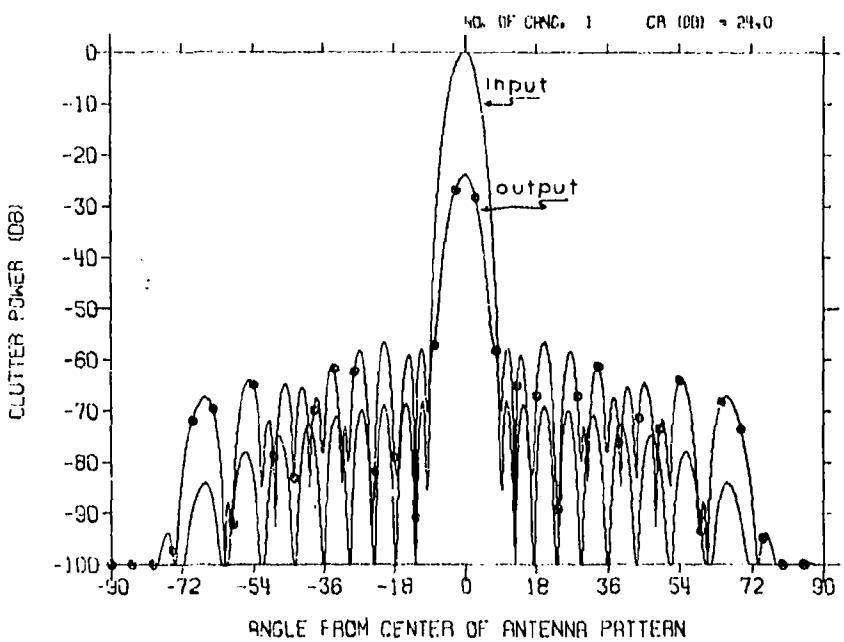

Fig. 16—Clutter power at the output and input of an MTI canceler with platform motion compensation using the correction pattern of Fig. 15 and the system parameters of Eqs. (34) and (36)

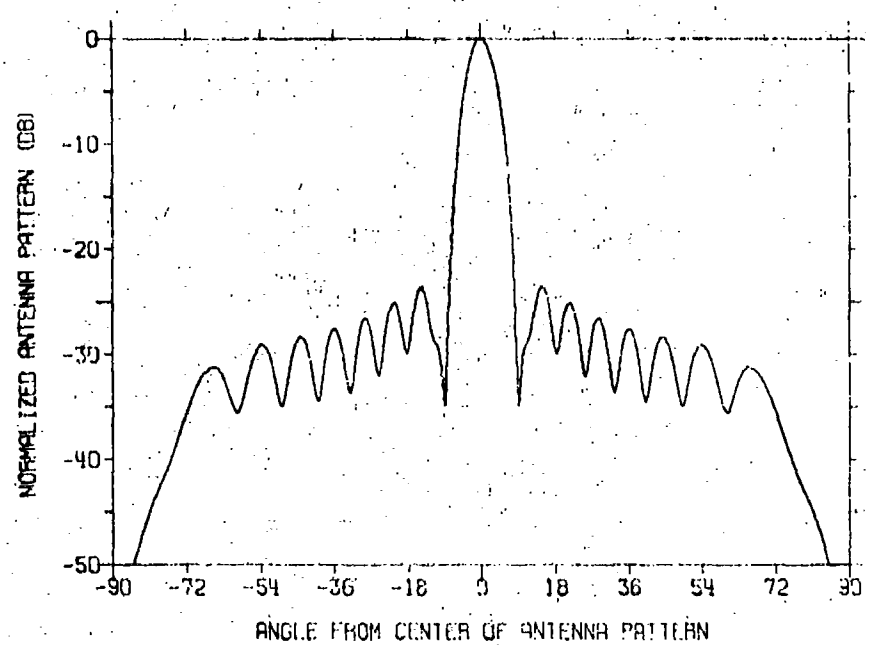

Fig. 17—Composite pattern representing the sum of the receive pattern of Fig. 14 and the correction pattern of Fig. 15

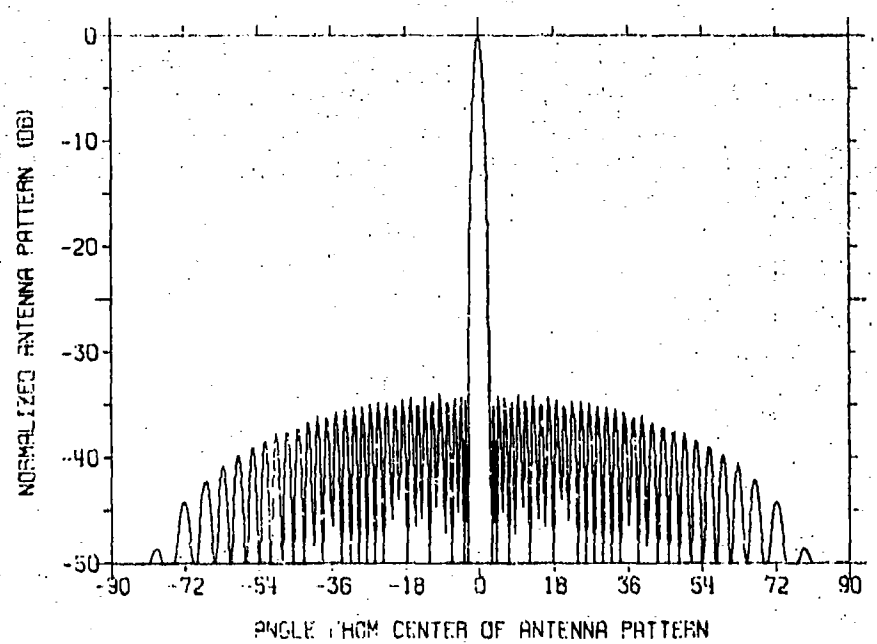

Fig. 18—Mean-squared antenna pattern for a 64-element array with dipole elements at 0.5-wavelength spacing and 34-dB Tschebyschev weights

The resulting weights are

$$(B'_{opt})_T = \begin{bmatrix} 0.625 & 0.0847 & 0.684 & 0.0392 \\ 0.529 & -0.0113 & 0.416 & -0.0495 \\ 0.337 & -0.0724 & 0.281 & -0.0813 \\ 0.243 & -0.0786 & 0.219 & -0.0676 \\ 0.205 & -0.0520 & 0.195 & -0.0351 \\ 0.188 & -0.0198 & 0.178 & -0.0086 \\ 0.165 & -0.0032 & 0.146 & -0.0046 \\ 0.121 & -0.0131 & 0.0891 & -0.0281 \\ 0.0519 & -0.0485 & 0.0106 & -0.0726 \\ -0.0332 & -0.0983 & -0.0772 & -0.124 \\ -0.119 & -0.146 & -0.157 & -0.163 \\ -0.189 & -0.174 & -0.212 & -0.176 \\ -0.226 & -0.169 & -0.230 & -0.153 \\ -0.221 & -0.131 & -0.200 & -0.106 \\ -0.154 & -0.111 & 0.0571 & 0.397 \\ -0.465 & 0.0631 & -0.306 & -0.570 \end{bmatrix} . \quad (42)$$

The weights corresponding to the second correction pattern are

$$b''_i = b'_{N-i+1} . \quad (43)$$

The correction pattern corresponding to the weights of Eq. (42) is shown in Fig. 19. The input and output clutter of an MTI canceler using these patterns, with Gaussian

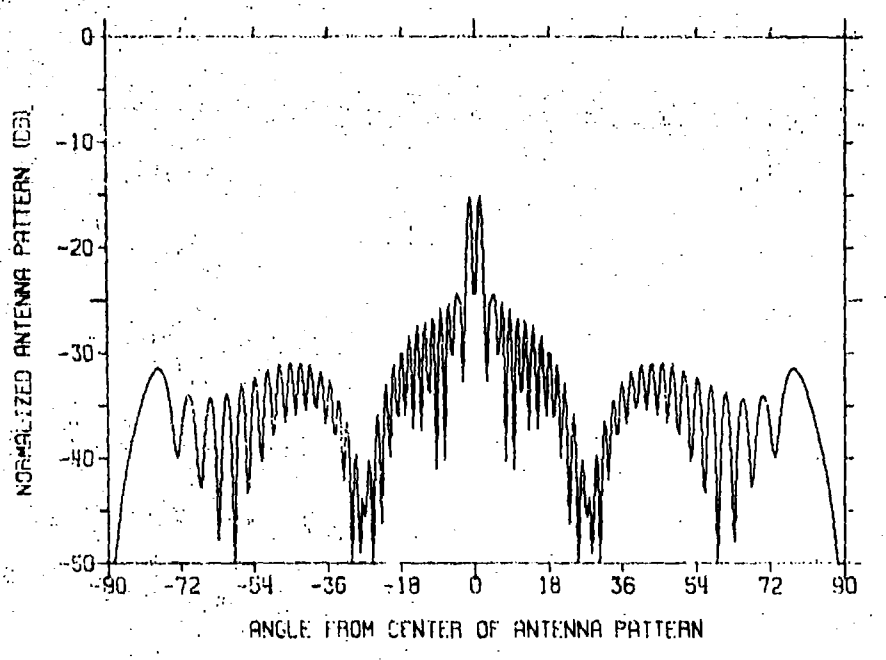

Fig. 19—Optimum platform motion correction pattern for the antenna pattern of Fig. 18 and the parameters of Eq. (34)

clutter defined by Eq. (36), are shown in Fig. 20. Again, the loss in main-lobe clutter cancellation is insignificant, and the sidelobe level is increased. The average clutter cancellation ratio is again dominated by the main-lobe clutter, and the loss is therefore insignificant.

Examination of Fig. 20 shows that the output clutter level in sidelobes very near the main lobe are especially increased. The composite pattern of Fig. 21 is the result of adding the correction pattern of Fig. 18 to the receive pattern of Fig. 19. The sidelobes very near the main lobe are very high, around −25 dB. Therefore, the clutter received through these composite sidelobes would be near the −50-dB level. Figure 20 shows that after cancellation, the clutter levels in these regions are higher than −60 dB. Therefore, less than 10 dB of cancellation is achieved in these sidelobes, much less than needed to overcome the higher level due to the correction pattern.

CONCLUSIONS

A method has been presented for designing platform motion correction patterns for AMTI radar systems. The procedure minimizes the total clutter residue of an AMTI averaged over all angles. The method is applied to four receive patterns (Figs. 3, 11, 14 and 18), and the corresponding correction patterns are derived (Figs. 8, 12, 15 and 19). The resulting clutter cancellation vs relationship angle for a Gaussian clutter spectrum whose standard deviation is 0.01 times the PRF is shown in Figs. 9, 13, 16 and 20.

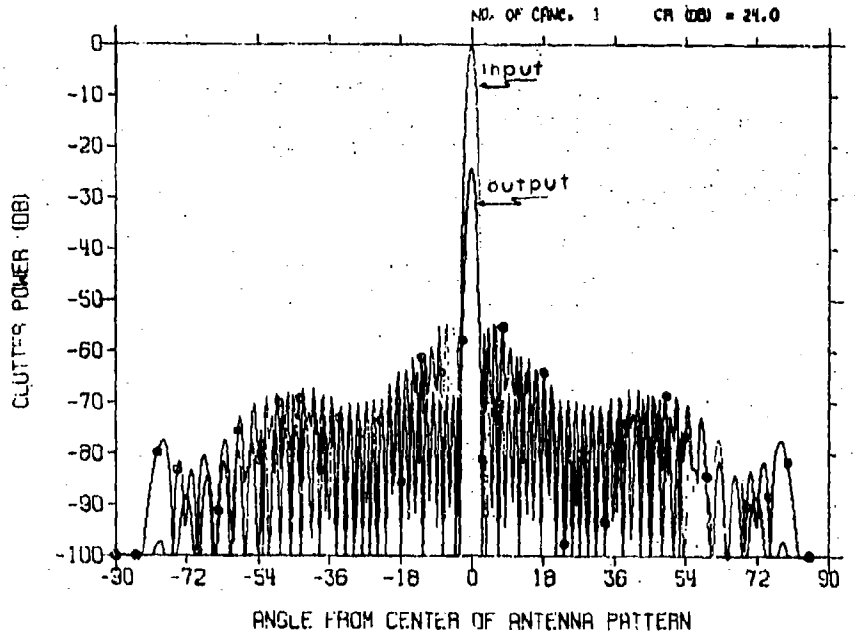

Fig. 20—Clutter power at the input and output of an MTI canceler with platform motion compensation using the correction pattern of Fig. 20 and the system parameters of Eqs. (36) and (41)

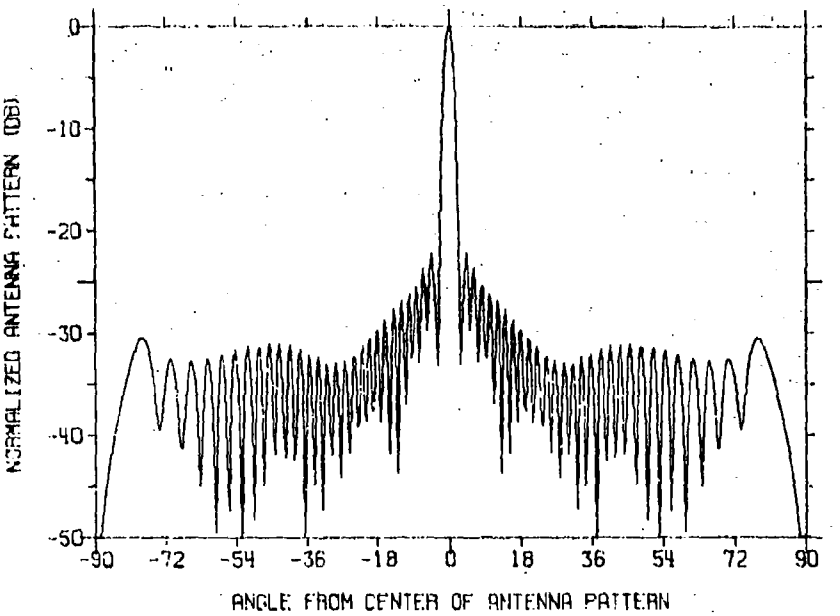

Fig. 21—Composite pattern representing the sum of the receive pattern of Fig. 18 and the correction pattern of Fig. 19

An MTI with no platform motion achieves a cancellation ratio of 24 dB against this clutter at all angles (Fig. 4). This ratio is achieved in the main lobe of all four sample antenna patterns (Figs. 9, 13, 16 and 20). However, the sidelobe clutter level increases at the MTI output in all four cases. For the three patterns whose sidelobe level is very low (−34 dB), the average clutter cancellation ratio is about 24 dB. Therefore, for these patterns, the loss of clutter cancellation due to platform motion is insignificant.

The technique summarized in Eqs. (30) and (32) provides a simple procedure for computing correction pattern weights. The equations are easily programed for solution on digital computers using conventional mathematical routines for integration and matrix algebra.

ACKNOWLEDGMENTS

I would like to thank Mr. David L. Ringwalt, Mr. Benjamin Koo, Mr. F. M. Staudaher, and Dr. Tomos L. ap Rhys, upon whose consultations this effort depended heavily. Special thanks are due Mrs. Rosalie Valentine for typing the manuscript.

REFERENCES

1. G. A. Andrews, "Optimal Radar Doppler Processors," NRL Report 7727, May 29, 1974.

2. G. A. Andrews, "Airborne Radar Motion Compensation Techniques: Evaluation of TACCAR," NRL Report 7407, Apr. 12, 1972.

3. F. R. Dickey, Jr., and M. M. Santa, "Final Report on Anti-clutter Techniques," General Electric Company, Heavy Military Electronics Dept., Report No. R65EMH37, Syracuse, N.Y., 1953.

4. "Final Engineering Report on Displaced Phase Center Antenna," vols. 1-3, Contract AF33(600)-24744, General Electric Company, Schenectady, N.Y., 1956-1957.

5. G. A. Andrews, "Airborne Radar Motion Compensation Techniques: Evaluation of DPCA," NRL Report 7426, July 20, 1972.